Title

Asymmetric Dual Arm Approach for Post Stroke Recovery of Motor Functions Utilizing the EXO-UL8 Exoskeleton System: A Pilot Study

Authors

Shen, Yang
Ma, Ji
Dobkin, Bruce
et al.

Publication Date

2018-05-10

Data Availability

The data associated with this publication are available upon request.

Peer reviewed

This article has been accepted for publication in Engineering in Medicine and Biology Society (EMBC), 2018 40th Annual International Conference of the IEEE. Citation information including DOI would be available once published on IEEE Xplore Digital Library.

Asymmetric Dual Arm Approach for Post Stroke Recovery of Motor Functions Utilizing the EXO-UL8 Exoskeleton System: A Pilot Study

Yang Shen[1], Ji Ma[1], Bruce Dobkin[2], and Jacob Rosen[1]

***Abstract*— In a dual arm therapeutic regime aiming to rehabilitate motor functions post stroke, both the affected arm (paretic) and the unaffected (non-paretic) arm are involved. In this context, the leading idea is that motor functions of the affected arm during a reaching task may be improved if the unaffected arm has already reached the target. As part of this pilot study, one chronic post-stroke patient with weakness and spasticity on his right arm conducted reaching tasks to virtual targets arranged in a 5×3 matrix located parallel to his frontal plane, in two different configurations: (1) affected arm only (without assistance from the exoskeleton); (2) unaffected arm first followed by the affected arm (2a) without, and (2b) with assistance. A force field attracting the wrist of the affected arm to the target was used in the assistive mode. The data post-processing and analysis included task completion time, reachable task space, joint range of motion, human-robot interaction force/torque and power exchange at multiple sensors along the arm - visualized in a series of interaction maps. The data validated the robotic system's basic functionality in facilitating post-stroke unilateral and asymmetric bilateral training. Future work would be expanded to clinical trials with more subjects to be recruited and additional features to be implemented.**

***Index Terms*— Rehabilitation robotics, upper-limb exoskeleton, dual-arm, physical human-robot interaction (pHRI), wearable robot, physical rehabilitation.**

I. Introduction

After a stroke, over 50% of persons have mild to severe weakness of the affected upper extremity that is managed by physical therapies to try to improve skillful arm and hand movements, strength, speed, and coordination [1], [2]. Automating rehabilitation training for the affected upper extremity by employing robotic systems has been proposed to increase the number of repetitions of exercise with more normal kinematics [3], [4], [5], [6], [7]. The devices are often categorized by the number of degrees-of-freedom (DOFs), either active or passive. Unlike single-DOF rehabilitation devices (e.g., manipulanda), exoskeletons for rehabilitation often involve physical human-robot interaction (pHRI) at multiple limb locations [8].

Control strategies for these exoskeletons include using surface electromyography (sEMG) signals, feedback from force and inertial sensors, and detection of electroencephalography (EEG) signals to activate motion. Understanding how a person physically interacts with rigid linkages becomes important especially for exoskeleton devices controlled by interaction forces only. Lower limb exoskeletons are usually developed for assisting standing and for walking, which is cyclic movement constrained by the ground and repetitive, rather stereotyped stance and swing phases of gait [9]. In contrast, arm rehabilitation training by upper limb exoskeletons must have more flexibility in protocol design to achieve reaching and grasping at a variety of locations in peripersonal space. The upper extremity exoskeletons must detect multi-joint movement intention as the person initiates a purposeful movement to an item. Hemiparetic persons are impaired by abnormal synergistic movements, hypertonicity, and variable motor control of flexor, extensor and rotator muscle groups. How they react to external assistance and resistance of an exoskeleton requires further study.

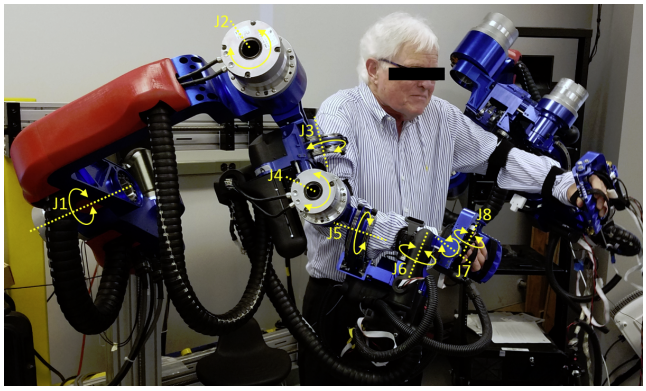

Fig. 1. The subject in this study is operating the EXO-UL8 upper limb exoskeleton system in dual arm mode (rotation axes of eight active DOFs on the right exoskeleton arm are marked in yellow).

In addition, there is little or no research on robotic systems that train ecologically valid movements in which the hands asymmetrically converge to interact with an object (e.g., to open a jar, button a shirt, prepare a meal, dress). Other than exoskeletons that enslave the affected arm to movements of the other arm, most devices enable practice with only the affected arm. An important conceptual basis for an asymmetric bilateral practice approach to recovery from hemiplegia is that when either hand purposefully holds an item, bilateral attentional mechanisms for the integration of motor, visual, spatial, sensory, motivational, and other cognitive-motor nodes of the central nervous system are activated. This added drive may increase training-induced problem-solving and activation of spared, distributed motor networks that can further support recovery of the paretic arm and hand. Thus, an important technological barrier

[1]Bionics Lab, Department of Mechanical and Aerospace Engineering, University of California Los Angeles, Los Angeles, CA 90095, USA yang_shen@engineering.ucla.edu, jima@ucla.edu, jacobrosen@ucla.edu

[2]Department of Neurology, the Neurologic Rehabilitation and Research Program, Geffen School of Medicine, University of California Los Angeles, Los Angeles, CA 90095, USA bdobkin@mednet.ucla.edu

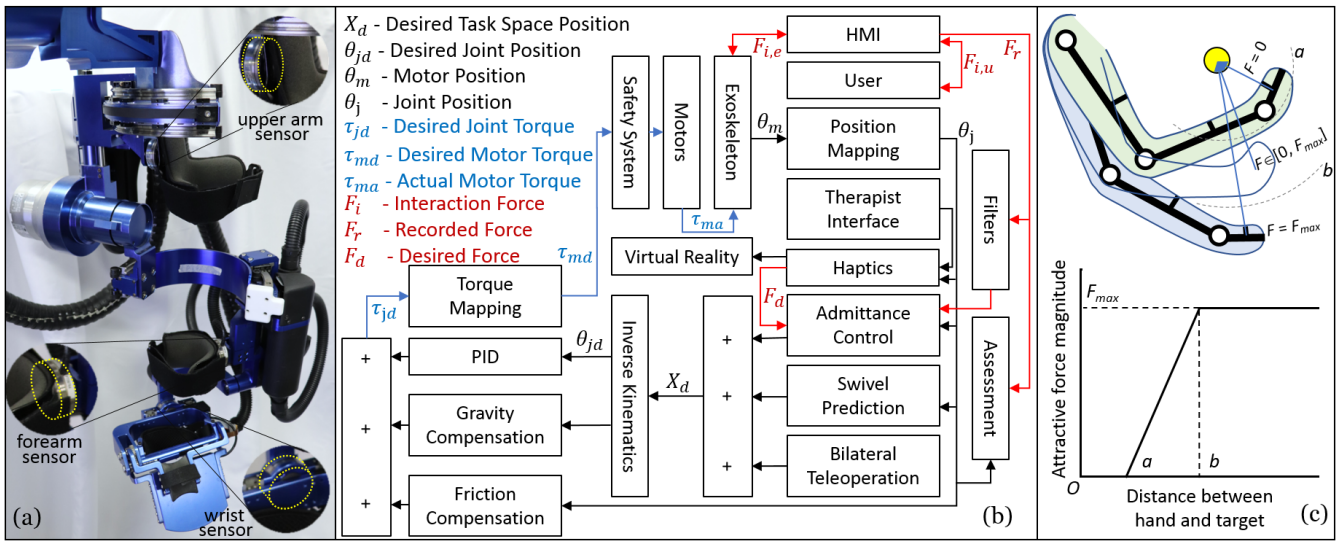

Fig. 2. EXO-UL8 dual-arm upper limb exoskeleton system: (a) F/T sensor positions - upper arm, forearm and wrist; (b) full view of controller - the core is admittance control; (c) exoskeleton could provide spring-like force assistance attracting hand to the target (maximum and minimum values saturated).

to more effective UE rehabilitation that deploys robotic-assist systems is the absence of control mechanisms and rehabilitation strategies to use one arm to help train the other for daily activities. We have altered our original design of this bilateral robotic system to enable this.

To explore more in pHRI when stroke patients are wearing exoskeleton, we conducted this very preliminary study. The rest of the paper is arranged as: Part II introduces the current exoskeleton system, EXO-UL8; Part III describes the experiment including multiple assessment tasks for one chronic stroke patient; Part IV provides quantitative results and analytical discussion including interaction visualization; Part V concludes the paper.

II. EXO-UL8 Upper Limb Exoskeleton System

A. Mechanical design

The new EXO-UL8 (Fig. 1), like its predecessor, the cable-driven EXO-UL7 [10], was designed to overlap with 95% of a healthy human arm workspace. The shoulder joint was designed to eliminate singular configurations within the workspace and was repositioned at the edge of the arm's workspace. Single-DOF hand grippers were added to increase the total number of DOFs from seven to eight for each arm and to enable reach-and-grasp motions that are critical to the recovery of the motor control system following a stroke. Furthermore, each link is adjustable in length in a telescopic fashion to accommodate a wide range of anthropometric arm dimensions (5% - 95%). Each joint includes mechanical limits preventing motion beyond anatomical limits. The cable driven mechanism embedded in the EXO-UL7 was replaced with servo unities mounted at each individual joint with two exceptions including the upper arm (J3) and forearm (J5) where belts were introduced. The servo system was selected to meet the combination of the following specs: (a) muscle strengths - provide joint torques that are comparable to a healthy individual; (b) gravity compensation - provide joint torques that compensate the weight of exoskeleton arm itself as well as that of the subject arm; (c) velocities/accelerations - provide angular velocities and accelerations comparable to those measured in activities of daily living; (d) payload - provide support of a payload of 5kg grasped by the hand. For each arm, three harmonic drive (Harmonic Drive Systems Inc., Japan) servo systems are equipped with encoders to facilitate movement for three out of the seven DOFs (J1, J2, J4 - Fig. 1) at the shoulder and elbow joints, and with brakes that can freeze the arm configuration. The remaining five DOFs (J3, J5, J6, J7, J8 - Fig. 1) are equipped with DC motors (Maxon Motor, Swiss). A set of four force/torque (F/T) sensors are placed at all the physical interaction points between the human operator and the exoskeleton system (Fig. 2(a)): three multi-axis F/T sensors (ATI mini 40) are located on the upper arm, forearm, and wrist, between a brace and the corresponding exoskeleton link; one single-axis force sensor is incorporated into the exoskeleton gripper for sensing grasping forces applied by the fingers. Anodized aluminum links are custom made and all cables are covered with 3D-printed shells.

B. Control

The exoskeleton system controller is illustrated in Fig. 2(b), adopted from [11]. The Jacobian matrices mapping the force/torque data collected by the sensors located on upper arm $J_{u(6\times3)}$, forearm $J_{f(6\times5)}$, and wrist $J_{w(6\times7)}$ to the base frame (center of shoulder joint) are calculated. From each sensor, force and torque signals ($F=[f_x,f_y,f_z,\tau_x,\tau_y,\tau_z]^T$) are picked up and transmitted to each joint in the form of joint torque command signals: $\Gamma_{j,u(3\times1)}=J^T_{u(3\times6)}F_{u(6\times1)}$, $\Gamma_{j,f(5\times1)}=J^T_{f(5\times6)}F_{f(6\times1)}$, and $\Gamma_{j,w(7\times1)}=J^T_{w(7\times6)}F_{w(6\times1)}$, respectively. Individual contributions are augmented with zero entries and summed up:

$$\Gamma_j=\Gamma_{j,u}+\Gamma_{j,f}+\Gamma_{j,w} \quad (1)$$

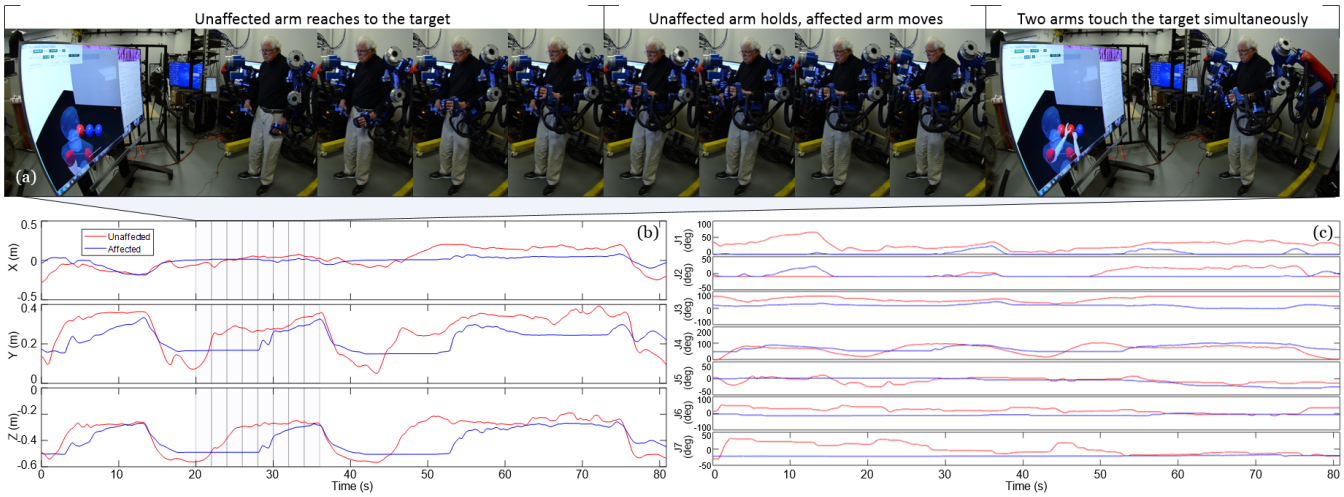

Fig. 3. (a) Experiment photos taken every two seconds (marked in (b)): the subject wearing EXO-UL8 is reaching to the second target in Task 3 (dual-arm mode, with assistance) - Level 1, full level kinematic information of which is shown in (b) wrist position change in task space and (c) joint position change of unaffected (red) and affected (blue) arms versus time.

The desired torque signals are filtered and fed into a PD admittance controller:

$$\dot{\theta}_j = k_{j,p}\Gamma_j + k_{j,d}\dot{\Gamma}_j \tag{2}$$

with the joint angular velocity signals $\dot{\theta}_j$ as the output to a low-level motor PID controller. The proportional and derivative gains for each DOF are tuned such that the human's effort reaches minimum while the system stability is maintained. There are two sources of instability in the system due to the physical human-machine interfaces: (1) human arm is assumed to be rigid enough to have every movement detected, but since the arm's cross-sectional shape is close to a circle, with muscles and skin surrounded, motions like wrist pronation/supination and shoulder internal/external rotation cannot be easily sensed by the F/T sensors; (2) human arm cross-section profile varies among individuals and loose/tight cuffs change detection sensitivity. To address these uncertainties and non-linearities, hyper gains $\alpha_{j,s}, j \in \{1,2,...,7\}, s \in \{u,f,w\}$ were introduced to improve natural multi-joint coordination.

$$\Gamma_j = \alpha_{j,u}\Gamma_{j,u} + \alpha_{j,f}\Gamma_{j,f} + \alpha_{j,w}\Gamma_{j,w} \tag{3}$$

or in a complete form (gripper DOF considered separately):

$$\begin{bmatrix} \Gamma_1 \\ \Gamma_2 \\ \Gamma_3 \\ \Gamma_4 \\ \Gamma_5 \\ \Gamma_6 \\ \Gamma_7 \end{bmatrix} = \begin{bmatrix} \alpha_{1,u}\Gamma_{1,u} + \alpha_{1,f}\Gamma_{1,f} + \alpha_{1,w}\Gamma_{1,w} \\ \alpha_{2,u}\Gamma_{2,u} + \alpha_{2,f}\Gamma_{2,f} + \alpha_{2,w}\Gamma_{2,w} \\ \alpha_{3,u}\Gamma_{3,u} + \alpha_{3,f}\Gamma_{3,f} + \alpha_{3,w}\Gamma_{3,w} \\ \alpha_{4,f}\Gamma_{4,f} + \alpha_{4,w}\Gamma_{4,w} \\ \alpha_{5,f}\Gamma_{5,f} + \alpha_{5,w}\Gamma_{5,w} \\ \alpha_{6,w}\Gamma_{6,w} \\ \alpha_{7,w}\Gamma_{7,w} \end{bmatrix} \tag{4}$$

The hyper gains αs are manually tuned, and the exoskeleton's gravity and friction are separately compensated.

C. Assistance

A majority of upper limb post-stroke training tasks include reach and reach-to-grasp. Due to the redundancy in both the arm and the robotic exoskeleton, only the end effector (hand) is provided with a point-to-point attractive force field so that elbow flexibility is maximized and the user's pHRI preference could be assessed. Illustrated in Fig. 2(c): when the distance between hand and target (either virtual or real object) is within $[a,b]$, the exoskeleton provides a spring-like attractive force field, which is saturated to the maximum F_{max} if the distance is over b, and eliminated if below a to main system controller stability. In this study, one set of a, b, and F_{max} (50mm, 200mm, 10N) is used.

III. Experiment

One chronic post-stroke patient (male, 75 years, 79kg, 175cm) with weakness and spasticity in his right arm was recruited, and he served as the test subject following an approved IRB protocol (IRB #17-001646). This pilot study focuses on the validation of EXO-UL8's functionality in facilitating single-arm and dual-arm training for post-stroke patients. Previously the difference between dominant and nondominant arm movements without wearing exoskeletons was broadly studied (e.g., [12]). We look more into the pHRI when post-stroke patients are wearing the upper limb exoskeleton system and the arms work separately as in real-world activities.

A. Setup

Fig. 3(a), 4(a) and 4(b) together provide an overview of the experiment setup: facing towards a wide screen, the subject wearing the EXO-UL8 moved his arms to accomplish tasks in virtual reality while standing. The exoskeleton shoulder distance and arm link lengths are adjusted for the subject's comfort. Joint angle information is transmitted to the virtual reality environment programmed with the open source haptic library Chai3D 3.0 via a UDP protocol [13]. The subject could thus control the virtual avatar in real-time, with no movement scaling. The subject receives auditory instructions

and visual feedback when accomplishing the tasks detailed below.

B. Tasks

Illustrated in Fig. 4(a) and (b), based on the subject's reachable task space measured using a ten-camera motion capture system (Vicon, UK), the targets are symmetrically (about the subject's sagittal plane) positioned in a 5×3 matrix parallel to the subject's frontal plane (500mm distant). The horizontal distance between columns is 210mm (half the subject's shoulder width), and vertical distance between rows (levels) is 100mm. Note that the second row from the top (Lv4) is the same height as the subject's shoulder. While the subject could easily reach all the targets using his unaffected (left) arm, targets on the matrix's top row and right column are partially reachable by the subject's affected (right) arm. The subject is asked to operate the exoskeleton for assessment of the following three different tasks:

Task 1 (affected arm only, no assistance): First, only the lowest row (Lv1) of the target matrix is displayed, and the subject, wearing exoskeleton, is asked to move his affected (right) arm to touch the left, center and right targets. Once touched the target changes color and the subject moves his arm back to the side. After all three targets are touched, the current task level disappears, the next higher level appears and the subtask continues. A short break is provided between each of the levels. A long break is provided after all five levels are attempted. The subject is asked to try his best to touch the target, and if he fails, relax the arm and move to the next. The exoskeleton does not provide any assistance.

Task 2 (unaffected $\rightarrow$ affected arm, no assistance): In this task, for each level (pattern and order same as Task 1) the subject moves the unaffected (left) arm to touch the target, which then changes to semi-transparent. While maintaining this position, he moves his affected arm to touch the same target. Once touched by two hands simultaneously, the target changes color. The subject retracts both arms back to his sides, then goes for the next target. No assistance provided by the exoskeleton.

Task 3 (unaffected $\rightarrow$ affected arm, with assistance): Similar to Task 2, except that once the unaffected (left) arm touches the target, the exoskeleton starts providing assistance in addition to voluntary movement, as illustrated in Fig. 2(c), to bring the hand to the virtual target. Once the target is touched by two hands simultaneously, the attraction force field disappears. Fig. 3 shows a sample target completion of Task 3 - Level 1.

C. Data collection

Both kinematic and force data are collected: joint position is recorded from the optical encoders at the seven motors on each exoskeleton arm at 100Hz; force/torque information $f_x, f_y, f_z, \tau_x, \tau_y, \tau_z$ is recorded from the three sensors on each exoskeleton arm at 100Hz as well. The data post-processing is done using MATLAB R2016b (MathWorks, USA). Fig. 3(b) provides an example of wrist position change in task space while Fig. 3(c) shows the joint space change, both

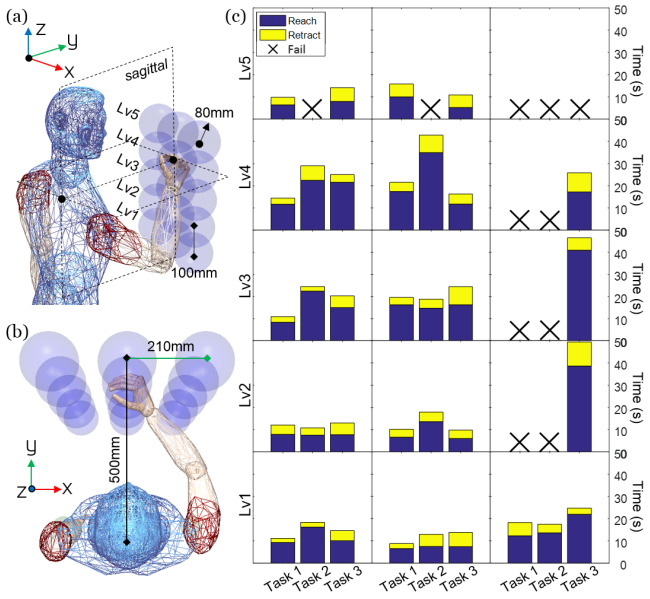

Fig. 4. (a) Virtual targets are arranged in a 5×3 matrix parallel to the subject's frontal plane. Each row represents a level, assuming difficulty increases from Lv1 to Lv5 since it requires the patient to lift the arm up; (b) top view of the subject and targets in virtual reality; (c) task completion of the affected (right) arm: reach time and retract time for each target, under each task and level. Targets failed to touch are marked in '$\times$'. All targets could be touched by the subject's unaffected (left) arm.

with respect to time. The full experiment process including subject, exoskeleton and VR display is recorded using a hi-res video camera equipped with a fisheye lens.

IV. Results & Discussion

Several aspects of the subject's physical interaction with EXO-UL8 are quantitatively analyzed and discussed below.

A. Kinematics

1) Task completion time: Unlike walking on the ground which is a cyclic movement with relatively constant rhythm, the completion time of reaching tasks often depends on the spatial position of targets because of weakness and slower coordination. The observed spatial heterogeneity in reach time shown in Fig. 4(c) (14.51 ± 9.07 second) reflects target-dependent task difficulty: a trend of increasing reach time from bottom-left to top-right indicates the spasticity, weakness and limited range of motion of the subject's affected arm. On the other hand, the retract time for different targets is much shorter and more concentrated (4.72 ± 2.06 second), due to the help from gravity and flexor synergy at the elbow and shoulder.

2) Reachable task space: Compared with single arm movement, dual-arm manipulation has a slightly reduced reachable workspace. As part of validation test, the subject confirmed the receipt of assistance from the exoskeleton. With the external assistance, even in dual-arm task mode the subject could reach more targets which need coordinated shoulder flexion and elbow extension. This matches the results found in our previous research using a manipulability model [14]. Another interesting observation (not plotted) is

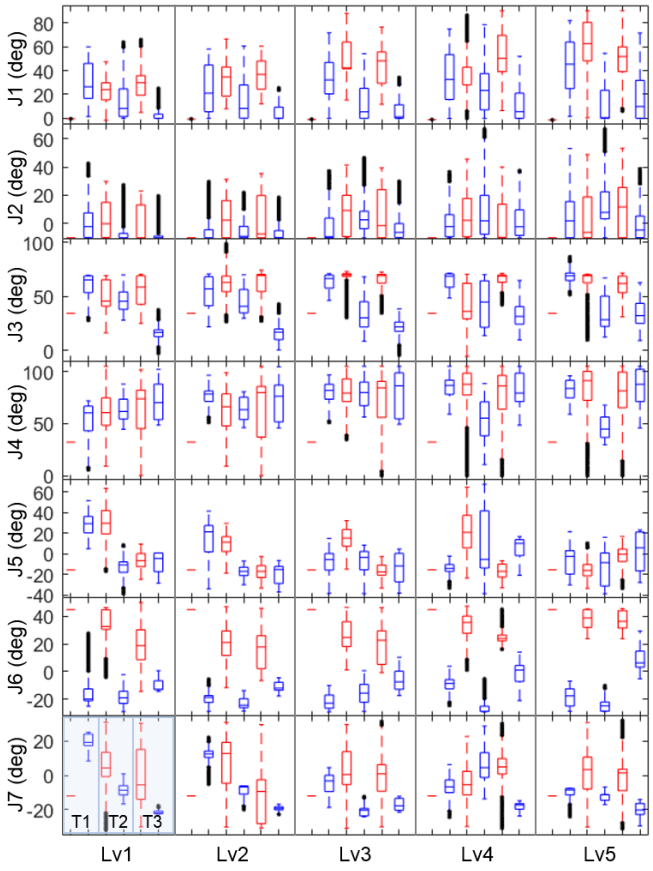

Fig. 5. Individual joint range of motion (ROM) distribution ('J·'). For each level ('Lv·'), six (6) boxplots represent three (3) tasks ('T·'): unaffected arm (Task 1, null - no movement), affected arm (Task 1), unaffected and affected arm (Task 2), unaffected and affected arm (Task 3). All unaffected ones are colored in red and affected are in blue.

that without additional instructions, the subject tended to rest his right arm and wait for assistance instead of trying to initiate the reach (rest period is not included in time calculation). More experiments should be done to validate the importance of assist-as-needed (AAN).

3) Joint space: For each task and level, the individual joint ROM is plotted in Fig. 5. The resultant rotation of J1-J3 is equal to that of the anatomical shoulder abduction(+) / adduction(-), shoulder flexion(+) / extension(-), and internal(+) / external(-) rotation; J4-J7 represent elbow flexion(+) / extension(-), forearm pronation(+) / supination(-), wrist extension(+) / flexion(-), radial(+) / ulnar(-) deviation. J8 is temporarily not included in this reach-only study (no grasp). Compared with the unaffected arm, the affected side is found to have more limited ROMs especially in forearm and wrist movements, possibly due to the subject's long-standing spasticity (Fig. 3(c) provides another view versus time). Besides J4 (elbow flexion/extension), no significant difference in the affected arm due to exoskeleton's assistance is observed. Unaffected arm fluctuation (when held at the target) is reduced when assistance is provided to the affected arm. We conjecture that this is due to regained attention. In future investigation, more assistive protocols (even for unaffected arm) would be added to the system for quantitative comparison, e.g., using the exoskeleton to freeze the unaffected arm's posture once it touches the target.

B. Physical human-robot interaction

1) Interaction maps: In many cases of human movement description and understanding, researchers analyze time-variant quantities like interaction forces with respect to time. Due to the existence of multiple sensors and links in contact with human arm, and in order to better depict the possible stroke-induced motion symptoms, a series of maps are visualized - for the trajectory of each sensor in task space, the corresponding temporal order, sensor force, torque, force- and torque-induced power are incorporated with colors to show the pHRI intensity (Fig. 6).

2) Forces and torques: High interaction forces and torques are observed in the upper arm sensor during reaching out movement (Fig. 6(b) and 6(c)). The average forces and torques illustrated in Fig. 7(a) and 7(b) indicate that the forearm sensor is less activated compared with other two sensors, for both unaffected and affected arm. This is possibly due to the null contact when the elbow is flexed and shoulder flexes to reach out. This *preference* of anatomical part usage suggests a dynamic change of hyper gains $\alpha_{j,s}$ based on user's arm configuration may be needed.

3) Power exchange: Visualized in Fig. 6(d-f), the interaction power consumed on each sensor includes force- and torque-induced (dominant) components, detailed calculation of which is provided in the Appendix. Since the admittance controller EXO-UL8 uses has, theoretically, a positive power exchange, the negative power (black) observed in part of the Fig. 6(a) trajectory indicates the exoskeleton links still have some inertia that needs to be compensated. We will fix this before further clinical trials. Note that the energy exchange (integral of power with respect to time) at the sensors is not the total energy consumed by the subject (e.g., isometric muscle contraction consumes energy as well). It is thus not plotted.

V. Conclusion & Future Plan

This pilot study discusses the mechanical and control of EXO-UL8, a dual-arm exoskeleton system for upper limb post-stroke rehabilitation. The device's functionality in facilitating single and dual-arm movement based on a chronic stroke patient's pHRI was validated while analyzing quantitative data such as task completion time, reachable workspace, joint ROMs, along with visualization of spacial interaction maps. Due to the force/torque distribution, the hyper gains αs may be further determined in dynamic movements, instead of being statically tuned. The proposed methodology will be further assessed with a larger pool of chronic post-stroke patients who will be recruited in future investigations.

Appendix

For readers' reference, the calculation of power exchange on distributed sensors $p_s, s \in \{u, f, w\}$ is provided below. The

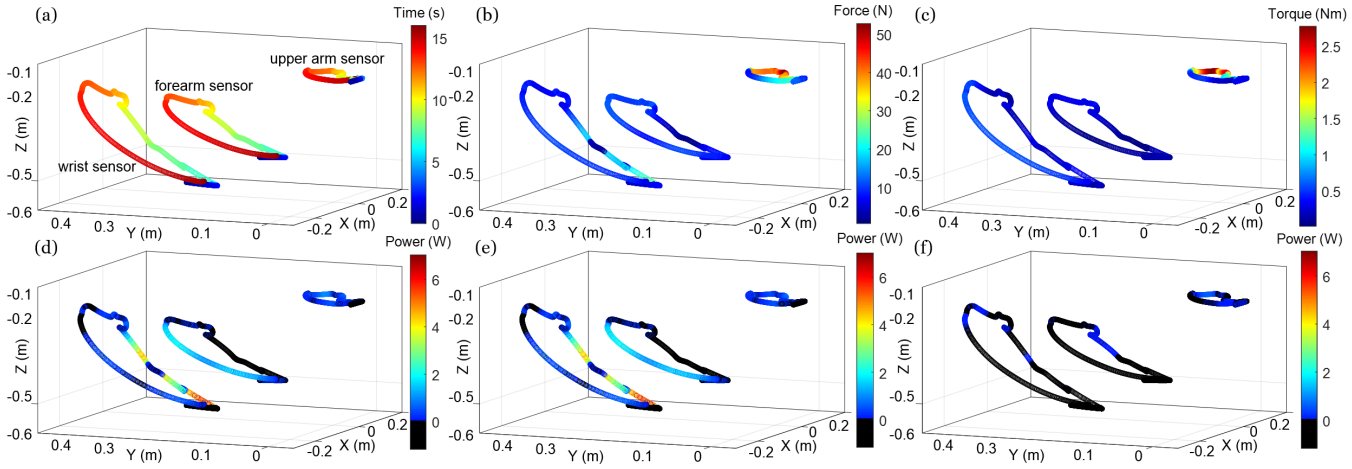

Fig. 6. Interaction maps of the affected (right) arm (movement trajectory in Fig. 3(a), Task 3-Level 1-Target 2, 20-36s) incorporated with colored information including: (a) temporal sequence; (b) interaction force ($\sqrt{f_x^2+f_y^2+f_z^2}$); (c) interaction torque ($\sqrt{\tau_x^2+\tau_y^2+\tau_z^2}$); (d) interaction power $p = p_f + p_\tau$; (e) force-induced interaction power p_f; (f) torque-induced interaction power p_τ. Note that the negative interaction power is shown in black.

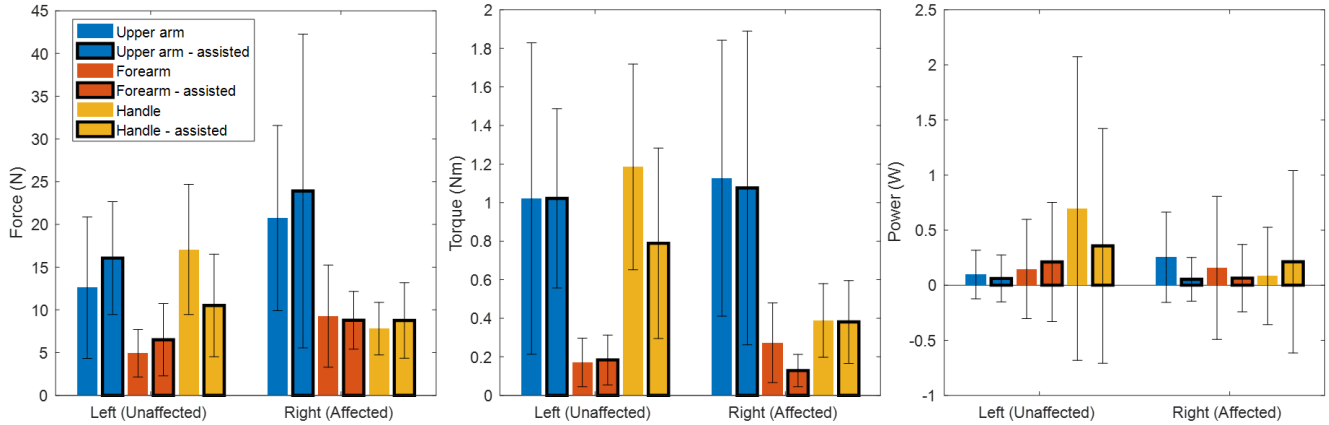

Fig. 7. Comparison of sensors on both arms, without (Task 2-Level 1) and with (Task 3-Level 1) assistance from the exoskeleton: (a) interaction force magnitude (mean ± std), (b) interaction force magnitude (mean ± std), (c) power p (mean ± std). Targets are the same since levels are the same.

ss in sub- and superscripts have different meanings, e.g., ${}^s\mathbf{v}_s$ is the linear velocity of sensor s in its local coordinate system, while ${}^0\mathbf{v}_s$ represents that in the global coordinate system which is fixed to the shoulder center. First, find the instantaneous homogeneous transformation matrix at time t:

$$ {}^0_sT(t+\delta t)_{(4\times4)} = {}^0_sT(t)_{(4\times4)}\,{}^t_{t+\delta t}T_{(4\times4)} \tag{5} $$

$$ {}^t_{t+\delta t}T_{(4\times4)} = {}^s_0T(t)_{(4\times4)}\,{}^0_sT(t+\delta t)_{(4\times4)} \tag{6} $$

$$ {}^t_{t+\delta t}T_{(4\times4)} = \begin{bmatrix} {}^t_{t+\delta t}R_{(3\times3)} & {}^t_{t+\delta t}\mathbf{P}_{(3\times1)} \\ \mathbf{0}_{(3\times1)} & 1 \end{bmatrix} \tag{7} $$

The local linear and angular velocities are calculated:

$$ {}^s\mathbf{v}_s(t) = \lim_{\delta t\to0} \frac{{}^t_{t+\delta t}\mathbf{P}_{(3\times1)}}{\delta t} \tag{8} $$

$$ \begin{bmatrix} 0 & -{}^s\omega_{s,z} & {}^s\omega_{s,y} \\ {}^s\omega_{s,z} & 0 & -{}^s\omega_{s,x} \\ -{}^s\omega_{s,y} & {}^s\omega_{s,x} & 0 \end{bmatrix} = \lim_{\delta t\to0} \frac{{}^t_{t+\delta t}R_{(3\times3)}}{\delta t} \tag{9} $$

$$ {}^s\boldsymbol{\omega}_s(t) = [{}^s\omega_{s,x}, {}^s\omega_{s,y}, {}^s\omega_{s,z}]^T \tag{10} $$

Power exchange p_s (positive means energy flows from human arm to sensor) on each sensor s consists of force- and torque-induced components calculated locally:

$$ p_{s,f} = \mathbf{f}^T({}^s\mathbf{v}_s) = [f_x, f_y, f_z][{}^sv_{s,x}, {}^sv_{s,y}, {}^sv_{s,z}]^T \tag{11} $$

$$ p_{s,\tau} = \boldsymbol{\tau}^T({}^s\boldsymbol{\omega}_s) = [\tau_x, \tau_y, \tau_z][{}^s\omega_{s,x}, {}^s\omega_{s,y}, {}^s\omega_{s,z}]^T \tag{12} $$

$$ p_s = p_{s,f} + p_{s,\tau} \tag{13} $$

ACKNOWLEDGMENT

The authors appreciate the helpful comments on experiments from Dr. Clarisa Martinez.

REFERENCES

[1] E. J. Benjamin, M. J. Blaha, S. E. Chiuve, M. Cushman, S. R. Das, R. Deo, S. D. de Ferranti, J. Floyd, M. Fornage, C. Gillespie, C. R. Isasi, M. C. Jiménez, L. C. Jordan, S. E. Judd, D. Lackland, J. H. Lichtman, L. Lisabeth, S. Liu, C. T. Longenecker, R. H. Mackey, K. Matsushita, D. Mozaffarian, M. E. Mussolino, K. Nasir, R. W. Neumar, L. Palaniappan, D. K. Pandey, R. R. Thiagarajan, M. J. Reeves, M. Ritchey, C. J. Rodriguez, G. A. Roth, W. D. Rosamond, C. Sasson, A. Towfighi, C. W. Tsao, M. B. Turner, S. S. Virani, J. H. Voeks, J. Z. Willey, J. T. Wilkins, J. H. Wu, H. M. Alger, S. S. Wong, and P. Muntner, "Heart Disease and Stroke Statistics-2017 Update: A Report From the American Heart Association," *Circulation*, vol. 135, no. 10, pp. e146–e603, mar 2017.

[2] B. H. Dobkin, "Rehabilitation after Stroke," *N. Engl. J. Med.*, vol. 352, no. 16, pp. 1677–1684, 2005.

[3] J. Klein, S. J. Spencer, J. Allington, K. Minakata, E. T. Wolbrecht, R. Smith, J. E. Bobrow, and D. J. Reinkensmeyer, "Biomimetic orthosis for the neurorehabilitation of the elbow and shoulder (BONES)," in *Biomed. Robot. Biomechatronics, 2008. BioRob 2008. 2nd IEEE/RAS-EMBS Int. Conf.*, 2008, pp. 535–541.

[4] S. Balasubramanian, Ruihua Wei, M. Perez, B. Shepard, E. Koeneman, J. Koeneman, and Jiping He, "RUPERT: An exoskeleton robot for assisting rehabilitation of arm functions," in *2008 Virtual Rehabil.* IEEE, aug 2008, pp. 163–167.

[5] T. Nef, M. Guidali, and R. Riener, "ARMin III - arm therapy exoskeleton with an ergonomic shoulder actuation," *Appl. Bionics Biomech.*, vol. 6, no. 2, pp. 127–142, 2009.

[6] T. Noda, T. Teramae, B. Ugurlu, and J. Morimoto, "Development of an upper limb exoskeleton powered via pneumatic electric hybrid actuators with bowden cable," in *Intell. Robot. Syst. (IROS 2014), 2014 IEEE/RSJ Int. Conf.*, 2014, pp. 3573–3578.

[7] M. H. Rahman, C. Ochoa-Luna, M. Saad, and P. Archambault, "EMG based control of a robotic exoskeleton for shoulder and elbow motion assist," *J. Autom. Control Eng.*, vol. 3, no. 4, pp. 270–276, 2015.

[8] N. Jarrassé, T. Proietti, V. Crocher, J. Robertson, A. Sahbani, G. Morel, and A. Roby-Brami, "Robotic exoskeletons: a perspective for the rehabilitation of arm coordination in stroke patients," *Front. Hum. Neurosci.*, vol. 8, no. December, p. 947, dec 2014.

[9] A. Rathore, M. Wilcox, D. Z. M. Ramirez, R. Loureiro, and T. Carlson, "Quantifying the human-robot interaction forces between a lower limb exoskeleton and healthy users," in *Eng. Med. Biol. Soc. (EMBC), 2016 IEEE 38th Annu. Int. Conf.*, 2016, pp. 586–589.

[10] J. C. Perry and J. Rosen, "Design of a 7 degree-of-freedom upper-limb powered exoskeleton," in *Biomed. Robot. Biomechatronics, 2006. BioRob 2006. First IEEE/RAS-EMBS Int. Conf.*, 2006, pp. 805–810.

[11] L. M. Miller, "Comprehensive control strategies for a seven degree of freedom upper limb exoskeleton targeting stroke rehabilitation," Ph.D. dissertation, University of Washington, 2012.

[12] C. Hansen, N. Rezzoug, P. Gorce, and B. Isableu, "Differences in the control of unconstrained three-dimensional arm motions of the dominant and the nondominant arm," *J. Appl. Biomech.*, vol. 32, pp. 311–315, 2016.

[13] F. Conti, F. Barbagli, R. Balaniuk, M. Halg, C. Lu, D. Morris, L. Sentis, J. Warren, O. Khatib, and K. Salisbury, "The CHAI libraries," in *Proc. Eurohaptics 2003*, 2003, pp. 496–500.

[14] Y. Shen, B. P.-Y. Hsiao, J. Ma, and J. Rosen, "Upper Limb Redundancy Resolution Under Gravitational Loading Conditions : Arm Postural Stability Index Based on Dynamic Manipulability Analysis," in *Humanoid Robot. (Humanoids), 2017 IEEE-RAS 17th Int. Conf.*, 2017, pp. 332–338.